ALPHA-PARTICLE PICKUP ON RARE-EARTH NUCLEI
WITH THE (d, 6Li) REACTION AT 35 MeV †

F. L. MILDER, J. JÄNECKE and F. D. BECCHETTI

Department of Physics, University of Michigan, Ann Arbor, Michigan 48109

Abstract: Spectra and angular distributions have been measured for the (d, 6Li) reaction on ^{138}Ba, ^{140,142}Ce, ^{142,144,146}Nd, ^{144,148,150,154}Sm and ^{166}Er using 35 MeV deuterons and magnetic analysis. Good agreement between measured and calculated angular distributions was obtained employing one-step zero-range distorted wave Born approximation (DWBA) theory with α-cluster wave functions. Alpha-particle spectroscopic factors S_α and reduced widths γ_α^2 have been extracted for the transitions to ground and excited states. Included in the analysis are earlier results for the (d, 6Li) reaction on ^{160}Dy, ^{208}Pb and ^{238}U. The spectroscopic factors range from approximately 0.002 to 0.1. The transitions to the ground states of nuclei with a few neutrons beyond $N = 82$ are enhanced. A close correspondence with the (p, t) two-neutron pickup reaction was observed. Several of the target nuclei are known α-particle emitters, and the direct comparison between reaction and decay data leads to a consistent description of these processes making it possible to deduce α-decay lifetimes and branching ratios from the (d, 6Li) data.

E

NUCLEAR REACTIONS ^{138}Ba, ^{140,142}Ce, ^{142,144,146}Nd, ^{144,148,150,154}Sm, ^{166}Er(d, 6Li), $E = 35$ MeV; measured $\sigma(E_{6Li}, \theta)$. ^{138}Ba, ^{140}Ce, ^{142}Nd, ^{144,154}Sm deduced S_α, reduced widths. ^{142}Ce, ^{144,146}Nd, ^{148,150}Sm, ^{166}Er deduced S_α, reduced widths, $T_{\frac{1}{2}}(\alpha)$. ^{160}Dy, ^{208}Pb, ^{238}U; analyzed previous data.

1. Introduction

Clustering phenomena in nuclei are presently of theoretical and experimental interest [1-5]. Of the many reactions and decays which provide experimental information about clustering, the (d, 6Li) and (^{3}He, ^{7}Be) α-particle pickup reactions have been used for many years [6] to investigate α-particle clustering in light and medium mass nuclei [6-9]. A recent survey [10] of (d, 6Li) reactions at $E_d = 35$ MeV on a variety of targets demonstrated the feasibility of using this reaction to study α-particle clustering over the entire mass range of nuclei. The (d, 6Li) cross sections were found to decrease approximately proportional to A^{-3}, but enhancements in certain regions such as the region of rare-earth nuclei were also observed. The mass region $138 \leq A \leq 166$ was therefore selected for a more systematic study. Preliminary results have been reported elsewhere [11].

Alpha-particle decay has long been used to study α-clustering in heavy nuclei [12, 13]. Alpha-particle transfer reactions extend these studies to all nuclei which are stable or nearly stable. The extraction of structure information from the α-decay process using

the standard R-matrix formalism [14-17]) is affected by its sensitivity to the α-particle binding energy via the penetrability factor and thus to the methods of calculating that penetrability. The analysis of α-cluster pickup reactions such as (d, ^{6}Li) and (^{3}He, ^{7}Be) is not influenced by this problem since the binding energy dependence of the transfer cross section is much weaker and well described by reaction theory [18]). However, the reaction analysis requires careful considerations related to the cluster wave function (form factor) and to the normalization both in zero-range as well as finite-range calculations. Transfer reactions probe the α-cluster wave function generally in a region near the nuclear surface, and α-particle reduced widths γ_α^2 extracted at a radius in this region should therefore be very reliable.

The reaction mechanism for the transfer of an α-particle is more complicated than that for the transfer of two nucleons. Nevertheless, if the structures of the initial and final states exhibit certain features, a correspondence between the two can be expected [19]). Furthermore, α-particle pickup reactions in the regions of rare-earth and translead nuclei [see also ref. [20])] offer an opportunity to compare reaction and α-decay data for ground as well as excited states. Three target nuclei which were studied here [including one from ref. [10])] are long-lived α-particle emitters.

The experimental procedure and results employed in this work are given in sect. 2. The DWBA analysis is presented in sect. 3. Sect. 4 includes the discussion of α-decay half-lives and branching ratios deduced from the (d, ^{6}Li) reaction. It also includes a comparison between α-particle and two-neutron pickup data [21-24]) and their interpretation on the basis of the pairing vibration model [25]).

2. Experimental procedures and results

The experiment was conducted with a 35.0 MeV deuteron beam from the University of Michigan 83 inch cyclotron. The targets consisted of rare-earth oxides evaporated onto carbon or nickel backings. They were typically 150 μg/cm^2 thick. The energy loss of the outgoing ^{6}Li particles in the target was the major contribution to the energy resolution of 60 to 90 keV. The resolution was adequate to separate most states of interest. The outgoing ^{6}Li particles were detected in two adjacent position sensitive solid state detectors mounted in the focal plane of a dispersion matched spectrometer. Details of the cyclotron system and the beam preparation and analyzing magnets have been previously reported [26]). The acceptance angle of the spectrometer was ±3° providing a solid angle of 2.0 msr. The ^{6}Li particles were completely stopped in the detectors resulting in energy signals from the detectors sufficient to cleanly separate the ^{6}Li ions from an intense background of lighter ions. Conventional electronics were used for data collection and on-line data reduction. Partially reduced data were stored in a PDP-15 computer as a two-dimensional array of ion position in the focal plane versus energy. The data were subsequently analyzed off-line.

A spectrum from the reaction ^{166}Er(d, ^{6}Li)^{162}Dy at $\theta_{lab} = 12°$ is shown in fig. 1. Indicated in the figure are four members of the ground-state rotational band in ^{162}Dy.

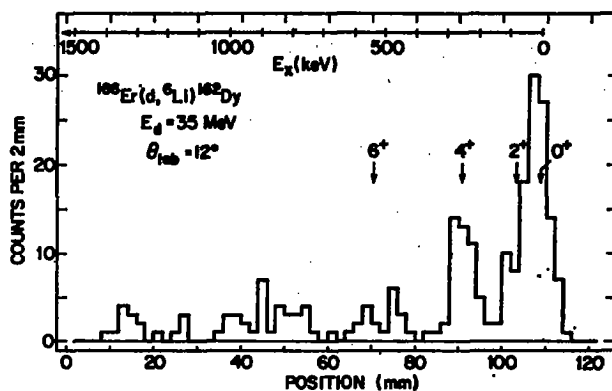Fig. 1. Spectrum of ^{6}Li particles from the ^{166}Er(d, ^{6}Li)^{162}Dy reaction at $\theta_{lab} = 12°$.
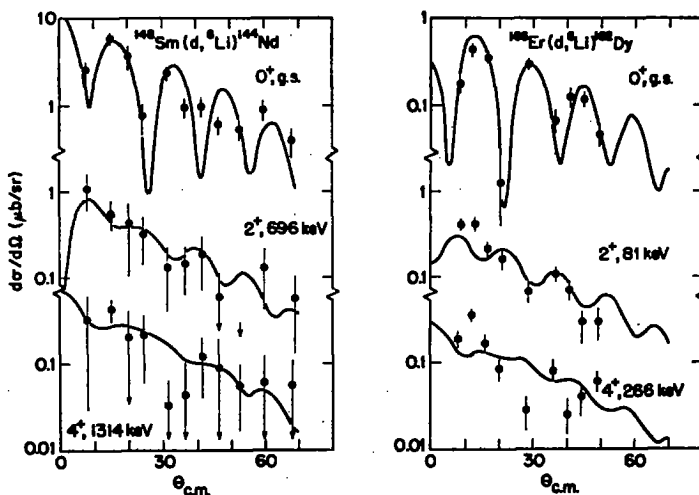

Fig. 2. Angular distributions for the transitions to the 0^+, 2^+ and 4^+ states in ^{144}Nd and ^{162}Dy from the (d, ^{6}Li) reaction on ^{148}Sm and ^{166}Er targets.

Transitions to higher excitation states can also be noted. These states could not be uniquely identified due to the limited resolution and the very small cross sections.

Angular distributions from $\theta_{lab} = 8°$ to $68°$ were measured on targets of ^{166}Er and ^{148}Sm (unless otherwise noted the reactions discussed will henceforth be identified by the target nucleus involved). The angular distributions along with the DWBA fits, which will be discussed later, are presented in fig. 2. More limited data were obtained on targets of ^{138}Ba, $^{140, 142}$Ce, $^{142, 144, 146}$Nd and $^{144, 150, 154}$Sm. In addition, we will include in the analysis and discussion data for ^{160}Dy, ^{208}Pb and ^{238}U from ref. [10]). Table 1 lists measured c.m. differential cross sections for the nuclei and states indicated. The cross sections quoted are for angles near the first $l = 0$

TABLE 1

Differential cross sections $d\sigma/d\Omega$ (first $l = 0$ maximum beyond 0°), absolute spectroscopic factors S_α and reduced widths γ_α^2 and θ_α^2 from the (d, ^{6}Li) reaction

Target nucleus	Residual nucleus	J^π	E_x (keV)	Q_α (keV)	$d\sigma/d\Omega_{c.m.}$ (μb/sr) (first maximum)	S_α	N^a)	$\gamma_\alpha^{2\,b}$) (keV)	$\theta_\alpha^{2\,b}$) ($\times 10^{-3}$)
^{138}Ba	^{134}Xe	0$^+$	0	−2576	1.85 ±0.31	0.031	8	0.23	1.07
		2$^+$	850	−3426	1.27 ±0.26	0.086	7	0.49	2.28
^{140}Ce	^{136}Ba	0$^+$	0	−1564	1.96 ±0.25	0.041	8	0.29	1.37
		2$^+$	818	−2382	1.03 ±0.18	0.067	7	0.38	1.79
^{142}Ce	^{138}Ba	0$^+$	0	1362	3.28 ±0.41	0.075	9	1.36	6.47
		2$^+$	1426	−64	0.21 ±0.10	0.011	8	0.15	0.71
^{142}Nd	^{138}Ce	0$^+$	0	− 805	4.44 ±0.42	0.078	8	0.54	2.57
		2$^+$	790	−1595	2.04 ±0.28	0.15	7	0.84	4.00
^{144}Nd	^{140}Ce	0$^+$	0	1902	6.10 ±0.44	0.060	9	1.00	4.80
		2$^+$	1596	306	0.92 ±0.24	0.018	8	0.21	1.01
^{146}Nd	^{142}Ce	0$^+$	0	1164	6.11 ±0.51	0.075	9	1.19	5.77
		2$^+$	641	523	0.59 ±0.16	0.013	8	0.14	0.68
^{144}Sm	^{140}Nd	0$^+$	0	−140	3.26 ±1.64	0.071	8	0.45	2.16
		2$^+$	774	−914	0.75 ±0.70	0.025	7	0.12	0.58
^{148}Sm	^{144}Nd	0$^+$	0	1974	5.56 ±0.64	0.078 ^{c})	9	1.20 ^{c})	5.88
		2$^+$	696	1278	0.52 ±0.19	0.010	8	0.13	0.64
		4$^+$	1314	660	0.40 ±0.12	0.013	7	0.037	0.18
^{150}Sm	^{146}Nd	0$^+$	0	1440	4.57 ±0.60	0.048	9	0.63	3.12
		2$^+$	454	986	0.39 ±0.18	0.016	8	0.17	0.84
^{154}Sm	^{150}Nd	0$^+$	0	−1213	0.42 ±0.10	0.009	9	0.062	0.31
		2$^+$	132	−1345	0.30 ±0.08	0.013	8	0.10	0.50
^{160}Dy ^{d})	^{156}Gd	0$^+$	0	154	1.43 ±0.18	0.032	9	0.22	1.14
^{166}Er	^{162}Dy	0$^+$	0	822	0.42 ±0.06	0.012	9	0.078	0.41
		2$^+$	81	741	0.39 ±0.06	0.008	8	0.047	0.25
		4$^+$	266	556	0.33 ±0.05	0.013	7	0.056	0.30
		6$^+$	549	273	0.11 ±0.03	0.033	6	0.090	0.14
^{208}Pb ^{d})	^{204}Hg	0$^+$	0	519	0.040±0.017	0.005	9	0.0047	0.029
^{238}U ^{d})	^{234}Th	0$^+$	0	4266	0.023±0.007	0.002	11	0.0031	0.021
		2$^+$	48	4218	0.014±0.006	0.003	10	0.0054	0.037
		4$^+$	160	4106	0.012±0.005	0.004	9	0.0047	0.032
		6$^+$	310 ^{e})	3956	0.014±0.006	0.004	8	0.0055	0.038

^{a}) Assumed number of radial nodes in the α-cluster wave function.

^{b}) Channel radius $s = (1.7$ fm$)A^{\frac{1}{3}}$ ($A =$ residual).

^{c}) Normalized such that $\gamma_\alpha^2(s)$ is the same for the (d, ^{6}Li) reaction and the α-decay of ^{148}Sm with $T_{\frac{1}{2}} = 8.0 \times 10^{15}$ y.

^{d}) Data from ref. [10]).

^{e}) $E_x = 310 \pm 20$ keV from ref. [10]).

maximum beyond $0°$. All target nuclei studied have an even number of both neutrons and protons, and the 0^+ states in the table are therefore all ground states. The 2^+, 4^+ and 6^+ states (where observed) are the first, second and third excited states, respectively.

3. Analysis

3.1. DISTORTED WAVE BORN APPROXIMATION (DWBA) ANALYSIS

A DWBA analysis of the data has been performed using the one-step zero-range computer code DWUCK [27]) with form factors taken to be simple α-cluster wave functions. Spectroscopic factors S_α and reduced widths γ_α^2 are then defined phenomenologically for α-particle pickup reactions on 0^+ targets by [28, 29])

$$\frac{d\sigma_{exp}(\theta)}{d\Omega} = \mathcal{N} \frac{S_\alpha}{2J+1} \frac{d\sigma^{DWBA}(\theta)}{d\Omega}, \tag{1}$$

$$\gamma_{\alpha L}^2(s) = \frac{\hbar^2 s}{2\mu} S_\alpha |R_L^{DWBA}(s)|^2. \tag{2}$$

Here, $d\sigma^{DWBA}(\theta)/d\Omega$ is the calculated DWBA cross section, $\mathcal{N}$ is a normalization factor, s is the channel radius, μ is the reduced α-particle mass, and $R_L^{DWBA}(r)$ is the radial part of the (normalized) form factor. Spectroscopic factors S_α are to be understood throughout this work as the model-dependent quantities defined above. Ideally, one should use instead spectroscopic amplitudes calculated from microscopic theories as in two-nucleon transfer reactions, for example.

The dimensionless reduced with $\theta_{\alpha L}^2(s)$ is defined [15, 30]) by

$$\theta_{\alpha L}^2(s) = \gamma_{\alpha L}^2(s)/\gamma_W^2(s), \tag{3}$$

where

$$\gamma_W^2(s) = 3\hbar^2/2\mu s^2 \tag{4}$$

is the Wigner limit [30−32]).

In the simple zero-range approximation used in the present analysis, the normalization factor $\mathcal{N}$ includes the overlap of ^{6}Li with an α-particle and a free deuteron [33]) as well as the strength of the effective deuteron–α-particle interaction. While a finite-range calculation is in principle free of factors such as $\mathcal{N}$, it requires a good knowledge of the ^{6}Li wave function. More importantly, however, it is not clear [34]) whether a conventional finite-range analysis without the inclusion of antisymmetrization effects [1,35]) should lead to correct absolute spectroscopic factors and reduced widths.

Both, zero-range as well as finite-range calculations may be affected by contributions from two-step mechanisms. A further justification for the use of the simpler zero-range approximation is provided by the independence of the normalization factor on the α-cluster potential well parameters (see subsect. 3.9).

3.2. OPTICAL MODEL PARAMETERS

The deuteron and ^{6}Li optical model parameters are listed in table 2. The deuteron

TABLE 2

Optical model parameters and "bound" state parameters

Particle	V (MeV)	r_r (fm)	a_r (fm)	W (MeV)	W' (MeV)	r_W (fm)	a_W (fm)	r_s (fm)
d	91.0	1.10	0.83		14.25	1.25	0.90	1.3
^{6}Li	240.0	1.30	0.65	14.0 a)		1.70	0.90	1.3
α-cluster	b)	1.30	0.73					1.3

The optical model potential was used in the form
$$U_{opt}(r) = -Vf(r, R_r, a_r) - iWf(r, R_W, a_W) + iW'4a_W(d/dr)f(r, R_W, a_W) + V_c(r, R_s),$$
with
$$f(r, R_x, a_x) = (1 + \exp[(r - R_x)/a_x])^{-1}, \qquad R_x = r_x A^{\frac{1}{3}}.$$
a) $W = 12.0$ MeV for Pb and U; see ref. [38]).
b) Adjusted to give correct α-particle binding or decay energy; see text.

parameters were taken from the work of Hinterberger et al. [36]) as modified by Lewis et al. [37]); the ^{6}Li parameters are from our work [38]) at 50.6 MeV. The inclusion of spin-orbit terms in the deuteron and ^{6}Li optical potentials was found to have a negligible effect on the calculated (d, ^{6}Li) angular distributions. Only the deep minima in the $L = 0$ distributions are filled in slightly. Spin-orbit terms were therefore disregarded.

3.3. FORM FACTORS FOR BOUND AND UNBOUND STATES

Microscopic calculations for spectroscopic amplitudes are not available. The form factors for nuclei with positive α-particle binding energies B_α ($B_\alpha = -Q_\alpha$; see table 1) were therefore taken to be simple α-cluster wave functions with a specified number of radial nodes bound in a Woods-Saxon plus Coulomb potential well. The radius and diffuseness parameters are included in table 2. These are the same parameters used by Sherman et al. [39]) in their analysis of the (α, 2α) reaction. The nuclear well depths were adjusted to fit the α-cluster binding energies.

A different procedure was adopted for those nuclei where the α-cluster is unbound. This includes the nuclei ^{148}Sm, ^{144}Nd and ^{238}U which are known α-emitters. Here, the target nucleus was viewed as an extremely narrow elastic scattering resonance of an α-particle plus the residual nucleus at the energy Q_α. Scattering theory [15-17, 40]) requires the elastic channel wave function $u(r) = rR(r)$ to be asymptotically equal to an irregular Coulomb function $G_L(kr)$. This boundary condition is sufficient to determine the potential well depth and the α-cluster wave function. However, the wave function for the unbound α-cluster cannot be normalized to unity as required by the DWBA analysis. As the wave function falls off rapidly, a reasonable procedure is to normalize within some large radius. For example, the wave function at the classical outer turning point (≈ 80 fm for ^{144}Nd + α) is smaller than its value in the nuclear interior by typically twenty orders of magnitude, and the exact radius used for the normalization is therefore unimportant. A cutoff radius of 20 fm was chosen

in the present work. At this radius the α-cluster wave function is about ten orders of magnitude smaller than in the interior. The α-cluster wave functions as well as the integrand of the DWBA radial integrals fall off very rapidly with increasing radius for these long-lived, quasi-bound states. The above method is therefore nearly exact, and it is not necessary to employ more complicated procedures sometimes used for transitions to short-lived unbound states, as in analysis of (d, p) reactions.

The above procedure for constructing an α-cluster wave function does not take into consideration antisymmetrization effects which may be important for the nuclear interior [1,35]). These effects will be reflected in our S_α values.

3.4. QUANTUM NUMBERS

In order to calculate DWBA form factors it is necessary to specify the quantum numbers for the α-cluster wave function. This was done throughout the analysis by using the harmonic oscillator relation

$$(2N+L)+(2n+l) = \sum_{i=1}^{4}(2n_i+l_i). \tag{5}$$

Here, n_i and l_i are the radial and angular momentum quantum numbers of the four nucleons which are picked up and N, L and n, l are correspondingly the quantum numbers for the relative and internal motion of the cluster. Assuming an internal 0s motion ($n = l = 0$) for the four nucleons in the α-particle, the total number of oscillator quanta $Q \equiv 2N+L$ is uniquely defined once the shell-model orbitals of the individual nucleons are specified [41]). The number of radial nodes N (radial quantum number) used in the calculation of the spectroscopic factors S_α are listed in table 1. They are based on the simplest shell-model predictions [42]) [see subsect. 3.8].

3.5. DWBA NORMALIZATION

Eqs. (1)–(4) make it possible to extract absolute values for S_α, $\gamma_{\alpha L}^2$ and θ_α^2 from the measured (d, ^{6}Li) cross sections provided the DWBA normalization factor $\mathcal{N}$ is known. A normalization constant of $\mathcal{N} = 2.67$ has been deduced by requiring that the reduced widths γ_α^2 determined from the lifetime of the α-decay of ^{148}Sm (see below) and from the (d, ^{6}Li) reaction on a ^{148}Sm target are the same. The above normalization factor has been used throughout this work but may not be valid for (d, ^{6}Li) reactions on much lighter or heavier target nuclei due to finite-range or other mass-dependent effects.

Absolute spectroscopic factors S_α and reduced widths γ_α^2 and θ_α^2 obtained from the preceeding analysis are summarized in table 1.

3.6. THE α-DECAY ANALYSIS AND PENETRABILITIES

For α-decay from 0^+ parent nuclei we define [12, 15-17, 43])

$$\Gamma_{\alpha L} = \hbar\lambda_{\alpha L} = 2\gamma_{\alpha L}^2(s)P_L(Q_\alpha, s), \tag{6}$$

$$\gamma_{\alpha L}^2(s) = \frac{\hbar^2 s}{2\mu}|R_L(s)|^2. \tag{7}$$

$$P_L(Q_\alpha, s) = \lim_{r\to\infty}\left[ks\left|\frac{rR_L(r)}{sR_L(s)}\right|^2\right] \tag{8}$$

Here, $\Gamma_{\alpha L}$ is the partial width and γ_L is the partial decay constant for the transitions to the ground or excited states in the daughter nucleus. The half-life $T_{\frac{1}{2}}$ is given by a sum over all decay channels, $\ln 2/T_{\frac{1}{2}} = \sum_L \lambda_{\alpha L}$. The quantity s is again the channel radius and μ the reduced α-particle mass, $P_L(Q_\alpha, s)$ is the penetrability at the energy Q_α, and $R_L(r)$ is the radial part of the α-cluster wave function. Furthermore, since $\gamma_{\alpha L}^2(s)$ must be the same for reaction and decay, we have

$$R_L(r) = \sqrt{S_\alpha}R_L^{\text{DWBA}}(r), \tag{9}$$

where $R_L^{\text{DWBA}}(r)$ is the radial part of the form factor in eq. (2).

Eqs. (6)–(8) make it possible to extract absolute values for S_α, γ_α^2 and θ_α^2 from a measured decay constant λ provided an accurate value for the penetrability P_L can be calculated. Four different procedures for calculating P_L are discussed below.

Disregarding possible antisymmetrization effects [35]), the α-cluster wave functions used as form factors for the DWBA calculations and the α-cluster wave functions required in the R-matrix formulation of α-decay satisfy the same differential equation [15, 17]). The boundary conditions for the two functions are different though. The former resonance state function has to be asymptotically equal to an irregular Coulomb function $G_L(kr)$ while the latter function (pure outgoing wave) has to be asymptotically equal to a Coulomb function of the form $G_L(kr)+iF_L(kr)$. However, at the chosen DWBA cutoff radius of 20 fm the regular Coulomb function $F_L(kr)$ is about thirty orders of magnitude smaller than $G_L(kr)$ and inside the cutoff radius the two solutions are for practical purposes identical. The DWBA form factor was therefore used to calculate penetrabilities according to eq. (8) (procedure (a)). For comparison, penetrabilities were also calculated with various approximations often used in the literature [12, 13, 44]) and compared to the results of procedure (a). Fig. 3 shows the ratio of the calculated $L = 0$ penetrabilities for the decay ^{148}Sm → ^{144}Nd $+\alpha$ as a function of the channel radius s. Procedure (d) represents the WKB approximation to a pure Coulomb potential. This is one of the most common prescriptions [44]). At the classical inner turning point of 8.1 fm for ^{144}Nd $+\alpha$, the penetrability is a factor of about ten too small. Procedure (c) is based on eq. (8) using a pure Coulomb potential and ignoring the nuclear potential. The result is somewhat better. Procedure (b), finally, represents the WKB approximation to the combined Coulomb
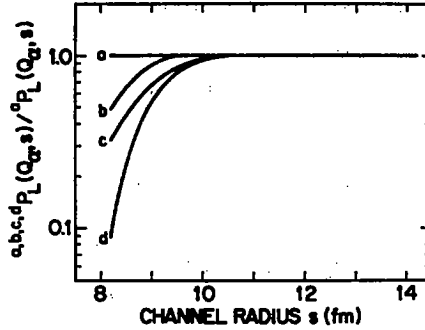
Fig. 3. Ratio of penetrabilities for the decay ^{148}Sm $\rightarrow$ ^{144}Nd$+\alpha$ as a function of channel radius. The penetrabilities were calculated (a) using wave functions generated in a nuclear and Coulomb potential, (b) using the WKB approximation with a nuclear and Coulomb potential, (c) using wave functions generated in a Coulomb potential only and (d) using the WKB approximation with a Coulomb potential only.

and nuclear potential. It differs at the small radii from the results of procedure (a) by a factor of two. As we are interested in reduced widths near the nuclear surface, procedure (a) was used for all calculations.

3.7. RELATIVE MERITS OF S_α AND γ_α^2 AND CHOICE OF CHANNEL RADIUS s

While both spectroscopic factors, S_α, and reduced widths, γ_α^2, can be deduced from the measured cross sections as outlined above, the former are much more model dependent than the latter. The reason is that the reaction probes only a certain limited region of the cluster wave function, generally near the nuclear surface. This is demonstrated by the radial dependence of the product of the form factor times the wave functions for the incoming and outgoing distorted waves. The product is strongly localized near the surface, particularly for the important contributions to the radial integral with $l \leq 15$. The spectroscopic factor is related to the entire wave function whereas the reduced width is essentially a measure of the wave function at one radius. Although the reduced widths contains correspondingly less information, it is significantly more reliable. This should be particularly true if the channel radius is chosen in the region where the α-cluster is actually picked up. In the (d, ^{6}Li) reaction on target nuclei with $A \approx 150$ at $E_d \approx 35$ MeV this corresponds to a channel radius $s = s_0 A^{\frac{1}{3}}$ with $s_0 \approx 1.7$ fm. This value was therefore used in the present work. Fig. 4a shows the radial dependence of the total probability distribution $u^2(r) = r^2 R^2(r) = 4\pi r^2 \psi^2(r)$ for the α-cluster in ^{144}Nd$+\alpha$. The average value in the interior region is indicated by a dashed line. Significant surface clustering is indicated even in this simple picture. The three points correspond to: (A) the radius at which the logarithmic derivative of the radial wave function vanishes [20]), $r_A = 7.50$ fm, (B) the inner classical turning point, $r_B = 8.12$ fm, (C) our channel radius $s = s_0 A^{\frac{1}{3}}$, $r_C = 8.91$ fm. Given a reliable model wave function, $\gamma_\alpha^2(s)$ [or $\theta_\alpha^2(s)$] can be extrapolated to larger or smaller radii by using eqs. (2) or (7). Fig. 4b shows the radial dependence of γ_α^2
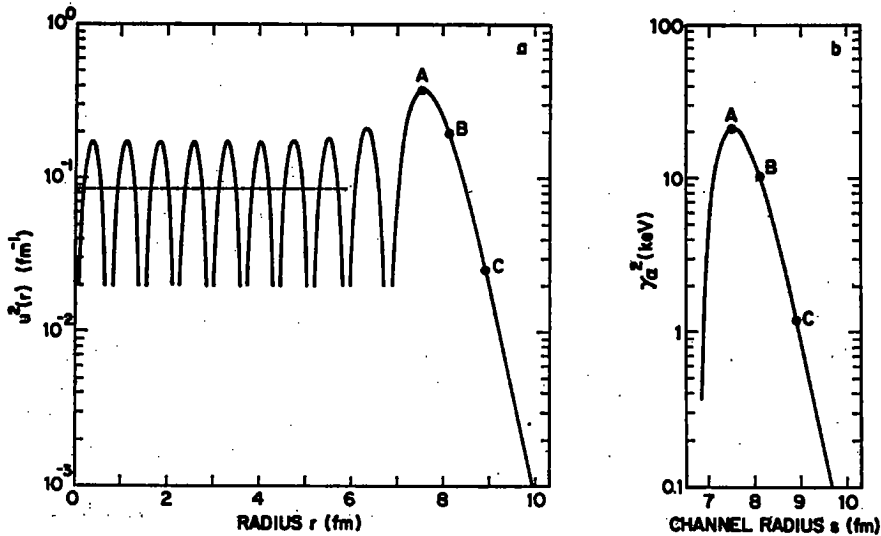
Fig. 4. (a) Plot of the quantity $u^2(r) = r^2 R^2(r) = 4\pi r^2 \psi^2(r)$ for the α-cluster wave function $\psi(r)$ of $^{144}\text{Nd}+\alpha$. The dashed line represents the average contribution in the interior region. (b) Plot of the reduced widths $\gamma_\alpha^2(Q_\alpha, s)$ for $^{148}\text{Sm} \to {}^{144}\text{Nd}+\alpha$ near the nuclear surface. The indicated radii are: (A) the radius where the logarithmic derivative vanishes, $(d/dr)\log \psi(r) = 0$, (B) the inner turning point, $V(r) = Q_\alpha$, and (C) the channel radius in the region where the α-particle is picked up in the (d, ^6Li) reaction, $s = (1.7 \text{ fm})A^{\frac{1}{3}}$.

in the surface region. However, the reliability of an extrapolation to smaller radii, particularly inside the inner classical turning point where antisymmetrization effects [1,35,34]) may dampen the wave function, depends strongly on the goodness of the α-cluster wave function. It should be noted that R-matrix theory does not require a particular channel radius or a particular boundary condition. The radius at which the logarithmic derivative vanishes is sometimes a convenient but not a required channel radius [eq. (2.1) in ref. [15])].

3.8. DEPENDENCE OF S_α AND γ_α^2 ON THE RADIAL QUANTUM NUMBER

The use of a single specified number N of radial nodes in the α-cluster wave function represents a simplification. Eq. (5) for the harmonic oscillator quantum numbers breaks down when Woods-Saxon wave functions are expanded in a harmonic oscillator basis. Moreover, contributions from proton pairs and/or neutron pairs in orbitals with different oscillator quantum numbers are generally present. The most important added contributions which will increase N for the cluster wave function of ^{148}Sm, for example, are $(0h_{\frac{9}{2}})^2$ for the protons and $(0i_{\frac{11}{2}})^2$ for the neutrons. A model wave function for ^{148}Sm was assumed to have the form $\psi(r) = A_9\psi_9(r) + A_{10}\psi_{10}(r)$ where A_9 and A_{10} have the characteristics of spectroscopic amplitudes. The normalized wave function $\psi_9(r)$ and $\psi_{10}(r)$ were generated using well depths adjusted to give nine and ten radial nodes, respectively at the same binding energy. They are

therefore not orthogonal; indeed $I \equiv \int \psi_9^*(r)\psi_{10}(r)d^3r \approx 0.34$. The calculated and experimental angular distributions of fig. 2 agree well over the entire range of constructive interference [$\psi(r)$ enhanced for large r] but only for small ($< 15 \%$) destructive admixtures of ten-node contributions. A pure nine-node form factor gives slightly better agreement (see fig. 2) than a pure ten-node form factor (not shown). The "spectroscopic factor" S_α defined [28]) by $S_\alpha = (A_9^2 + A_{10}^2 + 2A_9 A_{10} I)$ will depend strongly on the mixing ratio. (The factor containing the overlap integral I accounts for the lack in orthogonality.) As an example, if $A_{10} = 0$, then $S_\alpha = 0.078$ (table 1); if $A_9 = 0$, then $S_\alpha = 0.052$. Constructive interference (believed to prevail in the ground states), however, may lead to a value as small as $S_\alpha = 0.037$, whereas desctructive interference ($< 15 \%$) can lead to $S_\alpha = 0.20$. The strong variation of the spectroscopic factor is contrasted by the reduced width which remains essentially constant. The variation of γ_α^2 over the entire range of constructive interference is less than 2 %. and even for small destructive interference γ_α^2 does not change by more than 15 %.

3.9. DEPENDENCE OF S_α AND γ_α^2 ON THE α-CLUSTER POTENTIAL WELL PARAMETERS

A variation in the α-cluster Woods-Saxon potential well parameters r_0 and a leads to different reduced widths γ_α^2 and spectroscopic factors S_α. An uncertainty in the parameters will therefore result in an uncertainty of the spectroscopic quantities. Figs. 5a and b show the dependence of these quantities as extracted from the reaction data (solid lines) and decay (dashed lines) for ^{148}Sm as functions of r_0 and a. The channel radius was again taken as $s = (1.70 \text{ fm})A^{\frac{1}{3}}$ and the normalization factor as $\mathcal{N} = 2.67$. The graph shows that for all values of a and for $r_0 \gtrsim 1.3$ fm, both γ_α^2 and S_α scale very closely for reaction and decay. Thus, the comparison between the reaction and decay data is essentially independent of the choice of parameters. Similar results have been obtained in an analysis of the (^{16}O, ^{12}C) reaction on heavier nuclei [20]). The dependence of γ_α^2 on the parameters is several times weaker than that of S_α. Reaction and decay data deviate from each other for $r_0 < 1.3$ fm, but this region should be excluded anyway because of the strong disagreement between DWBA and experimental angular distributions. Fig. 5c, finally, shows the DWBA normalization factor $\mathcal{N}$ obtained from the condition that γ_α^2 is the same for reaction and decay and for *all* values of r_0 and a. Except for $r_0 < 1.3$ fm, $\mathcal{N}$ remains practically constant thus confirming the earlier conclusions which justify the use of the zero-range approximation in DWBA.

The reduced widths $\gamma_\alpha^2(s)$ of fig. 5a [$r_0 < 1.3$ fm excluded] were found to be strongly correlated with the potential $V(s)$ at the channel radius s [we find that the same is true for the reduced widths γ_α^2 of fig. 6 in ref. [20]) for the (^{16}O, ^{12}C) reaction on ^{208}Pb]. Fig. 6 shows the correlation (shaded area) plotted as a function of $V_{\text{nucl}}(s) = V(s) - V_{\text{Coul}}(s)$. This result is related to the "Igo ambiguity [45])" whereby low-energy elastic scattering depends essentially only on the potential in the tail region. Indeed, using the earliest Igo potential [46]) ($V_0 = 1100 \text{ MeV}, r_0 = 1.17 \text{ fm}, a = 0.574 \text{ fm}$), a reduced decay width of $\gamma_\alpha^2(s) = 0.65$ is obtained with the WKB approximation (open circle).
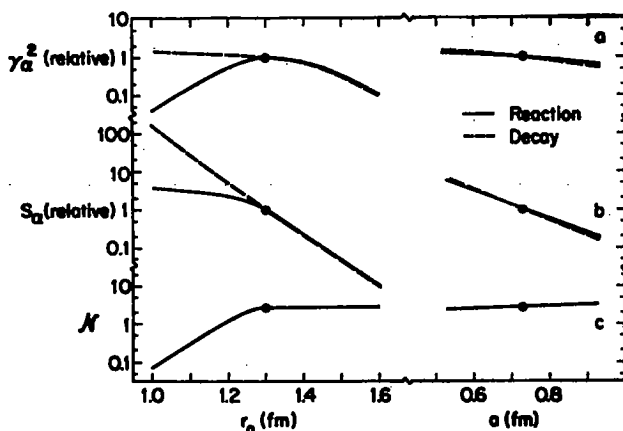
Fig. 5. Relative reduced widths (a) and spectroscopic factors (b) for the reaction ^{148}Sm(d, ^{6}Li)^{144}Nd and the decay ^{148}Sm → ^{144}Nd+α as a function of the α-particle potential well parameters r_0 and a. The filled circles correspond to the parameters $r_0 = 1.3$ fm and $a = 0.73$ fm. Part (c) shows the DWBA normalization factor needed to obtain the same reduced width for reaction and decay.
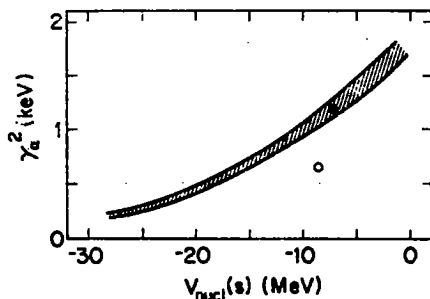

Fig. 6. Correlation between the reduced widths $\gamma_\alpha^2(s)$ at the channel radius $s = (1.7$ fm)$A^{\frac{1}{3}}$ for ^{148}Sm(d, ^{6}Li)^{144}Nd as well as ^{148}Sm → ^{144}Nd+α and the nuclear potential $V_{nucl}(s)$ obtained by varying the potential parameters. The filled circle corresponds to the adopted values r_0 and a, the open circle corresponds to the WKB decay value for one of the Igo potentials (see text).

Although the quantity $V_0 r_0^2$ for the above potential is almost 100 times larger than for the other potentials, the shape of the potentials in the surface region is sufficiently close to that of more realistic potentials and gives a reasonable decay width.

The foregoing discussion indicates that uncertainties in the potential parameters will not substantially affect the comparison between reaction and decay data. They lead to an uncertainty in the absolute reduced widths γ_α^2 by at most a factor of two.

4. Discussion

4.1. HALF-LIVES AND BRANCHING RATIOS

The consistency of the analysis has been checked by comparing the reduced widths and half-lives deduced from the measured (d, ^{6}Li) cross sections for the three long-

TABLE 3

Comparison of experimental α-decay half-lives $T_{\frac{1}{2}}$ and branching ratios β with values deduced from (d, ^{6}Li) reaction data for α-unstable target nuclei

Target parent	Residual daughter	J^π	E_x (keV)	Q_α (keV)	Reaction a) log $T_{\frac{1}{2}}$ (y)	β (%)	Decay b) log $T_{\frac{1}{2}}$ (y)	β (%)
^{142}Ce	^{138}Ba	0^+	0	1362	25.81	100		
		2^+	1426	c)				
^{144}Nd	^{140}Ce	0^+	0	1902	15.45	100	15.32±0.08	100
		2^+	1596	306		d)		unobserved
^{146}Nd	^{142}Ce	0^+	0	1164	35.00	100		
		2^+	641	523				
^{148}Sm	^{144}Nd	0^+	0	1974	15.90 a)	100	15.90±0.01	100
		2^+	696	1278				unobserved
		4^+	1314	660				unobserved
^{150}Sm	^{146}Nd	0^+	0	1440	28.34	100		
		2^+	454	986				
^{160}Dy e)	^{156}Gd	0^+	0	451	104.15	100		
^{166}Er	^{162}Dy	0^+	0	822	65.90	100		
		2^+	81	741		$\approx 2\times10^{-8}$		
		4^+	266	556				
		6^+	549	273				
^{208}Pb e)	^{204}Hg	0^+	0	519	129.72	100		
^{238}U e)	^{234}Th	0^+	0	4266	10.91	75	9.65±0.01	77±4
		2^+	48	4218		24		23±4
		4^+	160	4106		0.58		0.23±0.07
		6^+	310	3956		0.02		unobserved

a) Normalized such that $\gamma_\alpha^2(s)$ is the same for the (d, ^{6}Li) reaction and the α-decay of ^{148}Sm with $T_{\frac{1}{2}} = 8.0\times10^{15}$ y. Estimated uncertainty is ±1 in log $T_{\frac{1}{2}}$.

b) Data from refs. [48-51,61]).

c) ^{142}Ce cannot α-decay to excited states in ^{138}Ba.

d) Blank spaces indicate $\beta \ll 10^{-15}$ %.

e) Data from ref. [10]).

lived radioactive target nuclei ^{144}Nd, ^{148}Sm and ^{238}U with those derived from the decay data. Half-lives $T_{\frac{1}{2}}$ and branching ratios β were calculated from eq. (6) using the reduced widths of the DWBA analysis and exact penetrabilities (procedure (a) of fig. 3). The results are listed in table 3 together with the experimental [47-51,61]) half-lives $T_{\frac{1}{2}}$ and branching ratios β. The values for ^{148}Sm are, of course, identical having been used to extract the DWBA normalization constant $\mathcal{N}$. The agreement for ^{144}Nd is very good. Disagreement by a factor of about ten exists for the half-life of ^{238}U. The latter result should not be considered too disturbing as the reaction data [10]) are limited and the DWBA normalization factor $\mathcal{N}$ has been extrapolated over a wide range. Moreover, ^{238}U is a deformed nucleus and a proper treatment of the penetrability will reduce the calculated half-life. Similarly, an estimate using the same normalization factor $\mathcal{N}$ for (d, ^{6}Li) transitions in the 1p and 1d2s shells measured at the same deuteron energy [52,53]) implies small S_α values, e.g. $S_\alpha \approx \approx 0.02$ for ^{20}Ne(d,

^{6}Li)^{16}O. Again, due to the large extrapolation this result may not be accurate to better than an order of magnitude [the lowest order shell-model estimate [28]) is 0.23].

The values obtained for the branching ratios β in the decay ^{238}U → ^{234}Th + α are in very good agreement with the directly measured values [48]), particularly for the transitions to the 0$^+$ and 2$^+$ states. A comparison for the transition to the tentative 6$^+$ state [10]) at $E = 310 \pm 20$ keV is not possible as decay data are lacking for this state. The corresponding information for the reduced widths is included in fig. 9. Here, the ratios of the reduced widths of the excited states to that of the ground states are compared for the reaction and decay data, again in good agreement.

We estimate that the relative uncertainties of the reduced widths for the 0$^+$ states in the rare-earth nuclei are ± 30 %, mostly due to uncertainties in the target thicknesses. The uncertainties are increased for the 2$^+$ and particularly 4$^+$ and 6$^+$ states because of possible contributions from two-step processes. The absolute uncertainty is estimated at a factor of about three mostly due to the dependence on the α-cluster potential well parameters. The values for Pb and U may be about one order of magnitude too small as indicated by the comparison with the half-life of ^{238}U.

Table 3 includes the half-lives and branching ratios derived from the reaction data for all target nuclei with negative α-particle binding energies. These half-lives range up to 10^{129} y for ^{208}Pb. At present, such long half-lives cannot be measured directly. It should be noted that the half-lives so obtained follow approximately the predictions of the Geiger-Nutall relation [see fig. 7-3 in ref. [54])]

$$\log \lambda = \alpha - \beta Z Q_\alpha^{-\frac{1}{2}}, \tag{10}$$

with $\alpha = 55.5$ sec^{-1}, $\beta = 1.7037$ MeV$^{\frac{1}{2}} \cdot$ sec^{-1} or a similar semiempirical expression [55, 54]) and extend these relations to decay constants λ which are 100 orders of magnitude smaller than previously determined. Of course, the major contribution to eq. (10) arises from the penetrability factor of eq. (8). When its estimated uncertainty is combined with that for γ_α^2, we arrive at an estimated uncertainty of ±1 for $\log \lambda$ (y^{-1}) and $\log T_{\frac{1}{2}}$ (y).

4.2. ANGULAR DISTRIBUTIONS AND CROSS SECTIONS

Angular distributions for the (d, ^{6}Li) reaction on ^{148}Sm and ^{166}Er calculated with the DWBA computer code DWUCK [27]) and the optical and form factor parameters of table 2 are displayed in fig. 2. The ground-state distributions fit very well. However, the transitions to the 2$^+$ and most notably the 4$^+$ levels show more structure than the DWBA predictions. This fact suggests that multistep processes may be important for the transitions to the excited states similar [22, 56]) to the weak transitions to the excited 2$^+$ states observed in Nd(p, t). A coupled-channels analysis would therefore be desirable. The other feature which is immediately noticeable is the difference in magnitude of the cross sections for the two nuclei. The reaction on ^{148}Sm leads to a strong transition to the ground state of ^{144}Nd and considerably weaker transitions

to the excited states. The reaction on ^{166}Er, on the other hand, leads to weak transitions for all states in ^{162}Dy including the ground state. These states are all members of the ground-state rotational band.

4.3 GROUND-STATE TRANSITIONS

It is well known [12, 57, 58]) that simple shell-model estimates for the absolute α-particle reduced widths in heavy nuclei are one to three orders of magnitude smaller than those extracted from decay data. Attempts are being made [35]) to understand this discrepancy on the basis of antisymmetrization effects. Spectroscopic factors and possibly reduced widths extracted from decay and reaction data may also be affected by the required modifications in the cluster wave function and the form factor [34, 35]). Such effects are not considered in the present work.
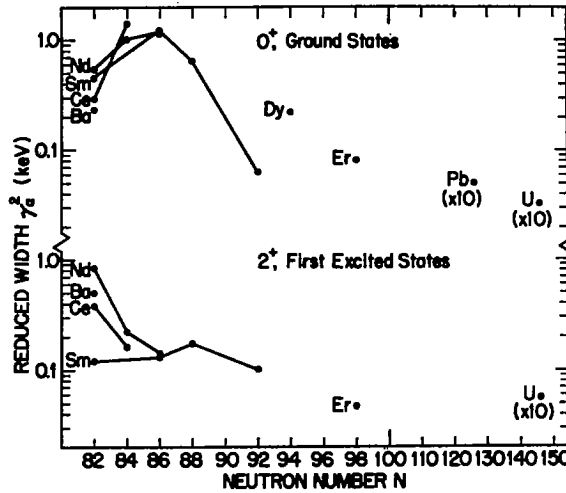

Fig. 7. Absolute α-particle reduced widths for (d, ^{6}Li) transitions to 0$^+$ ground states and 2$^+$ first excited states as a function of neutron number N.

Fig. 7 includes the measured reduced widths (table 1) for the transitions to the 0$^+$ ground states as a function of neutron number. The reduced widths increase considerably with the addition of a few neutrons to the closed shell at $N = 82$ followed by a strong reduction beyond $N = 88$. The small values for ^{208}Pb and ^{238}U are due to the choice of channel radius and possible uncertainties in the DWBA normalization as discussed earlier.

The reduced widths for $N = 82$ increase with proton number Z by a factor of two from $Z = 56$ (Ba) to $Z = 60, 62$ (Nd, Sm). There is a slight decrease for $N = 84$, and the two widths for $N = 86$ are about equal. The Z-dependence of α-particle reduced widths for even-Z nuclei with $N = 84$ has been treated theoretically many years ago [59]) on the basis of BCS theory with a simple pairing interaction. The

predicted minimum for $Z = 64$ was confirmed recently [60]) in a critical reevaluation of the α-decay data from $Z = 60$ to 72. Our results extend this sequence to $Z = 58$. The continued increase towards smaller Z-values disagrees with the predicted maximum at $Z = 60$. The Z-dependence of our results for the stable nuclei with $N = 82$ from $Z = 56$ to 62 agrees with the Z-dependence predicted [59]) for $N = 84$.

The increase of the reduced widths with N beyond $N = 82$ cannot be due to an additional node in the cluster wave function as required from shell-model considerations. The independence of the extracted widths to the assumed number of nodes has been demonstrated earlier.

It is evident from fig. 7 that the addition of a few neutrons past $N = 82$ makes the formation of an α-particle cluster in the surface region more probable. A similar but more pronounced effect has been observed near $N = 126$ for the reduced widths extracted for the polonium isotopes from the experimental α-decay half-lives [61]). It is also evident in the α-preformation probabilities obtained from studies of α-particle emission in (n, α) and (p, α) precompound nucleus reactions [62-64, 43]). The pronounced increase beyond the $N = 126$ shell for the polonium isotopes has been reproduced using simple harmonic oscillator wave function for the valence nucleons [65]) and also more sophisticated Nilsson wave functions with configuration mixing [12]).

Recent theoretical calculations [19]) predict a close connection between two-nucleon transfer and α-transfer reactions. It should manifest itself, for example, in the isotope dependence of (p, t) and (d, ^{6}Li) cross sections particularly when the neutron and proton pairs occupy different shell-model orbits. Indeed, this connection has been verified experimentally in a comparison between the (p, t) reaction [66, 67]) and the (d, ^{6}Li) reaction [10, 68]) on even-A and odd-A Sn isotopes. The protons transfered in the latter reaction behave essentially as a "spectator" pair. The connection between two-nucleon transfer and α-transfer reactions has also been observed [69]) in a comparison between (t, p) and (^{6}Li, d) transitions to several 0^+ states in ^{44}Ca. Also, for a number of fp shell ground-state transitions the (^{6}Li, d) α-transfer reaction was found [70]) to be related to the relevant (^{3}He, n) and (t, p) two-nucleon transfer reactions and in accord with the pairing vibration model [25]).

A similar comparison has now become possible for rare-earth nuclei. The (p, t) data for the Sm isotopes [23, 24]) and the Nd isotopes [21, 22]) are particularly useful. Differential cross sections for the (p, t) reaction on Sm and Nd isotopes are displayed in fig. 8 together with the (d, ^{6}Li) cross sections for the Sm and Nd isotopes. The cross sections are arbitrarily normalized to unity for the target nuclei with $N = 86$. The Sm(p, t) data are confirmed by the ground-state transitions observed in Sm(t, p) [ref. [71])], as is expected from the reciprocity theorem. The correspondence between the (d, ^{6}Li) and (p, t) ground-state transitions is striking except for $N = 92$. In particular, the broad maximum near $N = 86$ is confirmed. Calculations based on the pairing interaction model [72]) relate the cross sections of two-neutron transfer reactions between ground states to the pairing gap. The (p, t) data, now confirmed by (d, ^{6}Li) data, do not support the presence of a maximum at $N = 90$, as was already
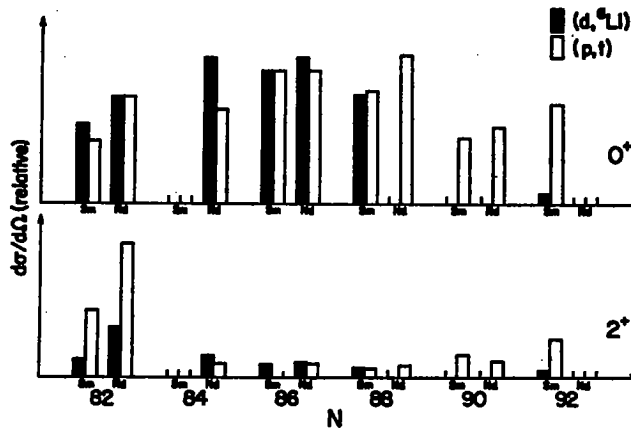
Fig. 8. Relative differential cross sections at the first maximum beyond 0° for the $L = 0$ and 2 angular distributions of Sm(d, ^{6}Li), Nd(d, ^{6}Li), Sm(p, t) and Nd(p, t). The data are normalized to unity at $N = 86$. The (d, ^{6}Li) data are for $E_d = 35.0$ MeV (this work); the Sm(p, t) data [24] are for $E_p = 25.5$ MeV; the Nd(p, t) data [21, 22] are for $E_p = 52$ MeV.

noted earlier [71, 23, 24]). The cross section for the ^{148}Sm(d, ^{6}Li)^{144}Nd ground-state transition is considerably weaker than expected from the comparison with the (p, t) data. This result is not too surprising since the correspondence in a sequence of isotopes requires the wave function for the transferred proton pair to be independent of the neutron configuration. The above transition, unlike transitions in the lighter isotopes, is one between strongly deformed states and the protons will likely take part in the collective motion of target and residual nucleus.

4.4. TRANSITIONS TO EXCITED STATES

Absolute reduced widths and differential cross sections for transitions to first excited 2^+ states are included in figs. 7 and 8, respectively. Fig. 9 shows the ratios of the excited state to ground state reduced widths as a function of neutron number N. The reaction and decay data [10, 48]) for ^{238}U are included. The inverse of the ratio of fig. 9 is related to the so-called reduced hindrance factor [61]).

The general behavior of the reduced width ratios of fig. 9 falls into three categories, (i) the semi-magic target nuclei with $N = 82$, (ii) the transitional nuclei with $84 \lesssim N \lesssim 88$, and (iii) the rotational nuclei with $N > 88$. The semi-magic nuclei ^{138}Ba, ^{140}Ce, ^{142}Nd and ^{144}Sm exhibit reduced widths for the 0^+ and 2^+ states which shift gradually in strength from the first excited 2^+ state to the 0^+ ground state. No explanation is offered except that the effect probably results from the influence of the proton orbitals on the structure of the final states.

The transitions to the first excited 2^+ states are very weak for all targets with $N = 84$, 86 and 88. The (d, ^{6}Li) and (p, t) results [22−24]) for the *entire* range $N = 82$
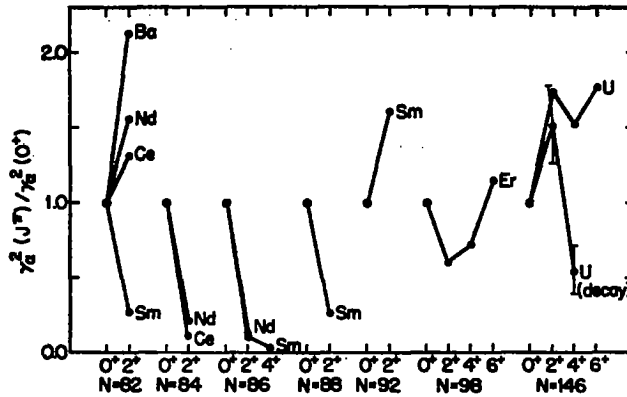
Fig. 9. Ratio of excited state to ground-state reduced widths from the (d, ^{6}Li) reaction. Decay values with uncertainties are included for ^{238}U.

to 88 are completely analogous. The close correspondence for the ground and first excited states is evident in the comparison of the differential cross sections of fig. 8. The weak ^{144}Sm(d, ^{6}Li)^{140}Nd(2$^+$) transition represents the only exception. It is worth noting that this weak transition and the rather strong ^{142}Nd(p, t)^{140}Nd(2$^+$) transition populate the same final state.

The strength of the (p, t) transitions to ground and excited states near $N = 82$ has been explained successfully [22-24] on the basis of the pairing vibration model [25]. Assuming zero-phonon ground states of the $N = 82$ nuclei, the addition or removal of neutron pairs with total angular momentum transfer of $L = 0$ leads to strong transitions between the ground states of the neighboring even isotopes. The lowest 2^+ states for $N < 82$ are removal-type quadrupole pairing vibration states. They are populated strongly in the pickup reaction. The lowest 2^+ states for $N > 82$ are addition-type quadrupole pairing vibrational states. They are populated only weakly in the pickup reaction and require a two-step reaction mechanism. Indeed, the weak transitions observed in Nd(p, t) have been successfully described in terms of coupled-channels Born approximation calculations [22]). The first excited 2^+ state for $N = 82$ is not a pairing vibrational state but presumably a particle-hole phonon state. It is populated weakly in pickup as well as stripping.

The relative strength of the transitions to the above 0^+ and 2^+ states can also be understood [73, 34]) on the basis of simple shell-model considerations. If one invokes the seniority model and assumes states of good seniority, the spectroscopic factors become related to quasi-spin coupling coefficients leading to conclusions similar to those from the pairing vibration model.

The reduced widths are approximately equal for the observed transitions to the ground and the excited states of all deformed nuclei studied, namely ^{148}Sm(d, ^{6}Li)^{144}Nd, ^{166}Er(d, ^{6}Li)^{162}Dy and ^{238}U(d, ^{6}Li)^{234}Th. The final states are all members of the ground-state rotational band. Such a behavior is quite reasonable

considering the fact that the internal structure of the excited states is very similar to that of the ground state, and that the space of contributing shell-model configuration is presumably large. One might therefore expect that the reduced widths decrease only slowly with increasing L.

A more complete analysis of the α-transfer data must await the development of suitable theoretical models or formalisms to calculate spectroscopic amplitudes from realistic wave functions. Boson-expansion methods, applied successfully [74] to the (t, p) stripping reactions [71] on $^{148, 150, 152}$Sm, for example, appear to be promising.

5. Summary

Reduced α-particle widths for long-lived radioactive rare-earth nuclei have been extracted from the (d, ^{6}Li) reaction and were found in accord with the reduced widths extracted from α-decay. This result has made it possible to deduce lifetimes for nearly stable α-particle unbound nuclei with $T_{\frac{1}{2}} > 10^{100}$ y.

While both absolute α-particle reduced widths γ_α^2 and spectroscopic factors S_α can be extracted from the measured cross sections, the former are far less model dependent than the latter. This property of the reduced widths is particularly pronounced when extracted at a channel radius which is close to the radius at which the α-particle is picked up in the (d, ^{6}Li) reaction. The absolute spectroscopic factors S_α for the rare-earth ground-state transitions range from about 0.01 to 0.10. The absolute reduced widths γ_α^2 extracted at a channel radius of $s = (1.7 \text{ fm})A^{\frac{1}{3}}$ range from about 0.1 to 1.0 keV.

The ground-state reduced widths increase significantly when a few neutrons are added to the closed shell at $N = 82$. Except for $N = 82$ the strength is strongly concentrated in the ground states for these nuclei. This behavior is very similar to that observed in two-neutron pickup reactions and can be understood in terms of the pairing vibration model. The widths for states in deformed nuclei are reduced as the total strengths are spread over members of the ground-state rotational bands.

References

1) K. Wildermuth and W. McClure, Cluster representations of nuclei, Springer Tracts of Modern Physics no. 41 (Springer, Berlin, 1966)
2) Int. Conf. on clustering phenomena in nuclei, Bochum, Germany, 1969 (IAEA, Vienna, 1969)
3) A. Arima, H. Horiuchi, K. Kubodera and N. Takigawa, Adv. in Nucl. Phys. 5 (1972) 345
4) Int. Symp. on cluster structure of nuclei and transfer reactions induced by heavy ions, Tokyo, 1975
5) D. A. Goldberg, J. B. Marion and S. J. Wallace, ed., Clustering phenomena in nuclei II, College Park, Maryland, 1975 USERDA Report ORO-4856-25 (1975)
6) L. J. Denes, W. W. Daehnick and R. M. Drisko, Phys. Rev. 148 (1966) 1097

7) P. Martin, J. P. Viano, J. M. Loiseaux and Y. Le Chalony, Nucl. Phys. A212 (1973) 304
8) G. Audi, C. Detraz, M. Langevin and F. Pougheon, Nucl. Phys. A237 (1975) 300
9) W. F. Steele, P. A. Smith, J. E. Finck and G. M. Crawley, Nucl. Phys. A266 (1976) 424
10) F. D. Becchetti, L. T. Chua, J. Jänecke and A. M. Vander Molen, Phys. Rev. Lett. 34 (1975) 225
11) F. L. Milder, J. Jänecke and F. D. Becchetti, in Clustering phenomena in nuclei II, ed. D. A. Goldberg, et al. USERDA Report ORO-4856-26 (1975) p. 409;
    F. L. Milder, Ph. D. thesis, The University of Michigan (1976) unpublished
12) H. J. Mang, Ann. Rev. Nucl. Sci. 14 (1964) 1
13) J. O. Rasmussen, in Alpha-, beta- and gamma-ray spectroscopy, ed. K. Siegbahn (North-Holland, Amsterdam, 1965)
14) E. P. Wigner and L. Eisenbud, Phys. Rev. 72 (1947) 24
15) A. M. Lane and R. G. Thomas, Rev. Mod. Phys. 30 (1958) 328
16) K. Takeuchi and P. A. Moldauer, Phys. Rev. C2 (1970) 925
17) A. Arima and S. Yoshida, Nucl. Phys. A219 (1974) 475
18) N. Austern, Direct nuclear reaction theories (Wiley-Interscience, New York, 1970)
19) D. Kurath and I. S. Towner, Nucl. Phys. A222 (1974) 1
20) W. G. Davies, R. M. DeVries, G. C. Ball, J. S. Forster, W. McLatchie, D. Shapira, J. Toke and R. E. Warner, Nucl. Phys. A269 (1976) 477
21) K. Yagi, Y. Aoki, J. Kawa and K. Sato, Phys. Lett. 29B (1969) 647
22) K. Yagi, K. Sato, Y. Aoki, T. Udagawa and T. Tamura, Phys. Rev. Lett. 29 (1972) 1334
23) P. Debenham and N. M. Hintz, Nucl. Phys. A195 (1972) 385
24) W. Oelert, G. Lindström and V. Riech, Nucl. Phys. A233 (1974) 237
25) A. Bohr, Proc. Int. Symp. on nuclear structure, Dubna (1968) p. 179;
    O. Nathan, ibid., p. 191
26) W. C. Parkinson, J. F. Peterson, R. H. Day, D. C. DuPlantis, W. S. Gray and J. Bardwick, Nucl. Instr. 119 (1974) 61
27) P. D. Kunz, University of Colorado, unpublished
28) M. Ichimura, A. Arima, E. C. Halbert and T. Terasawa, Nucl. Phys. A204 (1973) 225
29) A. Arima, R. A. Broglia, M. Ichimura and K. Schafer, Nucl. Phys. A215 (1973) 109
30) B. Buck, C. B. Dover and J. P. Vary, Phys. Rev. 11 (1975) 1803
31) J. B. Marion and F. C. Young, Nuclear reaction analysis (American Elsevier, New York, 1968) p. 86
32) A. Bohr and B. R. Mottelson, Nuclear structure, vol. 1 (Benjamin, New York, 1970) p. 441
33) V. G. Neudatchin, in Clustering phenomena in nuclei (IAEA, Vienna, 1969) p. 35
34) A. Arima, private communication, 1976
35) T. Fliessbach, Z. Phys. A272 (1975) 39;
    T. Fliessbach, H. J. Mang and J. O. Rasmussen, Phys. Rev. C13 (1976) 1318;
    T. Fliessbach and H. J. Mang, Nucl. Phys. A263 (1976) 75
36) F. Hinterberger, G. Mairle, V. Schmidt-Rohr, G. J. Wagner and P. Turek, Nucl. Phys. A111 (1968) 265
37) D. A. Lewis, A. S. Broad and W. S. Gray, Phys. Rev. C10 (1974) 2286
38) L. T. Chua, F. D. Becchetti, J. Jänecke and F. L. Milder, Nucl. Phys., to be published
39) J. D. Sherman, D. L. Hendrie and M. S. Zisman, Phys. Rev. C13 (1976) 20
40) J. R. Taylor, Scattering theory: The Quantum theory on non-relativistic collisions (Wiley, New York, 1972)
41) F. C. Chang, Phys. Rev. 137 (1965) B1420
42) M. Goeppert Mayer and J. H. D. Jensen, Elementary theory of nuclear shell structure (Wiley, New York, 1955)
43) S. Kadmenskii et al., Sov. J. Part. Nucl. 6 (1976) 189
44) E. K. Hyde, I. Perlman and G. T. Seaborg, The nuclear properties of the heavy elements, vol. 1 (Prentice Hall, Englewood Cliffs, New Jersey, 1964) p. 241
45) G. Igo, Phys. Rev. 115 (1959) 1665
46) G. Igo, Phys. Rev. Lett. 1 (1958) 72
47) R. B. Leachman and H. N. Schmitt, J. Nucl. Eng. 4 (1957) 38
48) G. E. Kocharov, A. P. Komar and G. A. Korolev, JETP (Sov. Phys.) 9 (1959) 48

49) J. Steyn and E. N. E. Strelow, Proc. Symp. on metrology of radionuclides, Vienna (IAEA, Vienna, 1960)

50) A. Isola and M. Nurmi, Z. Naturf. 20A (1965) 541

51) V. A. Korolev, G. D. Alkhazov, A. A. Vorobyev, A. K. Egorov and L. M. Vasilyeva, Sov. J. Nucl. Phys. 8 (1969) 131

52) A. M. Vander Molen, J. Jänecke and F. D. Becchetti, in Clustering phenomena in nuclei II, ed. D. A. Goldberg *et al.*, USERDA Report ORO-4856-26 (1975) p. 413;
A. M. Vander Molen, Ph.D. Thesis, The University of Michigan (1976) unpublished

53) J. D. Cossairt, R. D. Bent, A. S. Broad, F. D. Becchetti and J. Jänecke, Nucl. Phys. A261 (1976) 373

54) P. Marmier and E. Sheldon, Physics of nuclei and particles, vol. 1 (Academic Press, New York, 1969) p. 302

55) R. Taagepera and M. Nurmia, Ann. Acad. Sci. Fennicae: Ser. A VI (1961) no. 78, 1

56) T. Udagawa, T. Tamura and T. Izumoto, Phys. Lett. 35B (1971) 129

57) D. H. Wilkinson, Proc. Rutherford Jubilee Int. Conf. ed. J. B. Birks (Heywood, London, 1961) p. 339

58) J. K. Poggenburg, H. J. Mang and J. O. Rasmussen, Phys. Rev. 181 (1969) 1697

59) R. D. Macfarlane, J. O. Rasmussen and M. Rho, Phys. Rev. 134 (1964) B1196

60) W.-D. Schmidt-Ott and K. S. Toth, Phys. Rev. C13 (1976) 2574

61) J. O. Rasmussen, Phys. Rev. 113 (1959) 1593

62) L. Milazzo-Colli and G. M. Baraga-Marcazzan, Nucl. Phys. A210 (1973) 297

63) R. Bonetti and L. Milazzo-Colli, Phys. Lett. 49B (1974) 17

64) L. Milazzo-Colli, G. M. Baraga-Marcazzan, M. Milazzo and C. Signorini, Nucl. Phys. A218 (1974) 274

65) H. J. Mang, Phys. Rev. 119 (1960) 1069

66) D. G. Fleming, M. Blann and H. W. Fulbright, Nucl. Phys. A163 (1971) 401

67) D. G. Fleming, M. Blann, H. W. Fulbright and J. A. Robbins, Nucl. Phys. A157 (1970) 1

68) F. D. Becchetti and J. Jänecke, Phys. Rev. Lett. 35 (1975) 268

69) R. R. Betts, H. T. Fortune, J. N. Bishop, M. N. I. Al-Jadir and R. Middleton, Phys. Lett. 62B (1976) 37

70) R. R. Betts, in Clustering phenomena in nuclei II, ed D. A. Goldberg *et al.*, USERDA Report ORO-4856-26 (1975) p. 458

71) J. H. Bjerregaard, O. Hansen, O. Nathan and S. Hinds, Nucl. Phys. 86 (1966) 145

72) S. Yoshida, Nucl. Phys. 33 (1962) 685

73) A. de-Shalit and I. Talmi, Nuclear shell theory (Academic Press, New York, 1963)

74) D. Braunschweig, Nucl. Phys. A240 (1975) 457